Pramana – J. Phys. (2019) 92:84
https://doi.org/10.1007/s12043-019-1751-1

A novel approach via mixed Crank–Nicolson scheme and differential quadrature method for numerical solutions of solitons of mKdV equation

ALI BAŞHAN

Department of Mathematics, Science and Art Faculty, Zonguldak Bulent Ecevit University, 67100 Zonguldak, Turkey
E-mail: alibashan@gmail.com

MS received 28 June 2018; revised 5 November 2018; accepted 16 November 2018; published online 30 March 2019

Abstract. The purpose of the present study is to obtain numerical solutions of the modified Korteweg–de Vries equation (mKdV) by using mixed Crank–Nicolson scheme and differential quadrature method based on quintic B-spline basis functions. In order to control the effectiveness and accuracy of the present approximation, five well-known test problems, namely, single soliton, interaction of double solitons, interaction of triple solitons, Maxwellian initial condition and tanh initial condition, are used. Furthermore, the error norms L_2 and L_∞ are calculated for single soliton solutions to measure the efficiency and the accuracy of the present method. At the same time, the three lowest conservation quantities are calculated and also used to test the efficiency of the method. In addition to these test tools, relative changes of the invariants are calculated and presented. After all these processes, the newly obtained numerical results are compared with results of some of the published articles.

Keywords. Partial differential equations; differential quadrature method; mKdV equation; solitons; quintic B-splines.

PACS Nos **02.30.Jr; 02.30.Mv; 02.60.x; 02.60.Cb**

1. Introduction

Many physical phenomena are described via partial differential equations (PDEs). For this reason, a lot of researchers have investigated the solution of PDEs [1–5].

One of the most famous nonlinear differential equation known as the Korteweg–de Vries equation (KdV) equation in its simplest form is given by

$$U_t + \varepsilon U U_x + \mu U_{xxx} = 0, \tag{1}$$

where subscripts x and t denote partial derivatives with respect to space and time, respectively, and ε and μ are constant parameters.

The KdV equation stems from the study of shallow water waves [6] derived by Korteweg and de Vries to describe shallow water waves of long-wavelength and small-amplitude travelling in canals. It has been proved earlier that this equation has solitary waves as solutions, and hence it can have any number of solitons [7]. The equation has been the simplest nonlinear equation describing two important effects: nonlinearity which is represented by UU_x and linear dispersion which is represented by U_{xxx}. The nonlinearity of UU_x tends to localise the wave whereas dispersion spreads the wave out. The stability of solitons is a result of the delicate equilibrium between the two effects of nonlinearity and dispersion [8–11].

One of the most important KdV-type equation is known as modified KdV (mKdV) equation which was first introduced by Miura [12] and is given as follows:

$$U_t + \varepsilon U^2 U_x + \mu U_{xxx} = 0. \tag{2}$$

The mKdV equation has many physical applications in a wide range of areas such as electrodynamics, electromagnetic waves, elastic media, traffic flow [13,14], fluid dynamics [15,16] and plasma physics [17]. Various methods are used to obtain solutions of the KdV equation [18–21]. Both numerical and analytical solutions of the mKdV equation have been investigated by many researchers [22–30].

Differential quadrature method (DQM) was first introduced by Bellman *et al* [31] to obtain the numerical solution of PDEs. Many researchers have developed different types of DQMs utilising various base functions such as Legendre polynomials and spline functions [31,32], Hermite polynomials [33], radial basis functions [34], harmonic functions [35], Sinc functions [36,37], B-spline functions [38–40] and modified B-spline functions [41–43].

In this work, quintic B-spline-based Crank–Nicolson DQM (QCN-DQM) is going to be applied to obtain numerical solutions of the mKdV equation.

2. Quintic B-spline DQM

Let us take the grid distribution $a = x_1 < x_2 < \cdots < x_N = b$ of a finite interval $[a, b]$ into consideration. Provided that any given function $U(x)$ is smooth enough over the solution domain, its derivatives with respect to x at a grid point x_i can be approximated by a linear summation of all the functional values in the solution domain, i.e.

$$U_x^{(r)}(x_i) = \frac{\mathrm{d}^{(r)}U}{\mathrm{d}x^{(r)}}|_{x_i} = \sum_{j=1}^{N} w_{ij}^{(r)} U(x_j),$$
$$i = 1, 2, \ldots, N, \quad r = 1, 2, \ldots, N-1, \tag{3}$$

where r denotes the order of the derivative, $w_{ij}^{(r)}$ represent the weighting coefficients of the rth-order derivative approximation and N denotes the number of grid points in the solution domain. Here, the index j represents the fact that $w_{ij}^{(r)}$ is the corresponding weighting coefficient of the functional value $U(x_j)$. We need the first- and the third-order derivatives of the function $U(x)$. Therefore, we are going to find the value of eq. (3) for $r = 1$ and 3.

Let $Q_m(x)$ be the quintic B-splines with knots at points x_i where the uniformly distributed N grid points are taken as $a = x_1 < x_2 < \cdots < x_N = b$ on the ordinary real axis. In that case, the B-splines $\{Q_{-1}, Q_0, \ldots, Q_{N+2}\}$ form a basis for functions defined over $[a, b]$. The quintic B-splines $Q_m(x)$ are defined by the following relationships:

$$Q_m(x) = \frac{1}{h^5}\begin{cases} (x-x_{m-3})^5, & x \in [x_{m-3}, x_{m-2}], \\ (x-x_{m-3})^5 - 6(x-x_{m-2})^5, & x \in [x_{m-2}, x_{m-1}], \\ (x-x_{m-3})^5 - 6(x-x_{m-2})^5 + 15(x-x_{m-1})^5, & x \in [x_{m-1}, x_m], \\ (x-x_{m-3})^5 - 6(x-x_{m-2})^5 + 15(x-x_{m-1})^5 \\ -20(x-x_m)^5, & x \in [x_m, x_{m+1}], \\ (x-x_{m-3})^5 - 6(x-x_{m-2})^5 + 15(x-x_{m-1})^5 \\ -20(x-x_m)^5 + 15(x-x_{m+1})^5, & x \in [x_{m+1}, x_{m+2}], \\ (x-x_{m-3})^5 - 6(x-x_{m-2})^5 + 15(x-x_{m-1})^5 \\ -20(x-x_m)^5 + 15(x-x_{m+1})^5 - 6(x-x_{m+2})^5, & x \in [x_{m+2}, x_{m+3}], \\ 0, & \text{otherwise}, \end{cases}$$

where $h = x_m - x_{m-1}$ for all m [44].

Using the quintic B-splines as test functions in the fundamental DQM, eq. (3) leads to the equation

$$\frac{\partial^{(r)} Q_m(x_i)}{\partial x^{(r)}} = \sum_{j=m-2}^{m+2} w_{i,j}^{(r)} Q_m(x_j),$$
$$m = -1, 0, \ldots, N+2, \ i = 1, 2, \ldots, N. \tag{4}$$

An arbitrary choice of i leads to an algebraic equation system

$$M_1 W_1 = \Phi_1, \tag{5}$$

where $Q_{i,j}$ denotes $Q_i(x_j)$,

$$M_1 = \begin{bmatrix} Q_{-1,-3} & Q_{-1,-2} & Q_{-1,-1} & Q_{-1,0} & Q_{-1,1} & & & \\ & Q_{0,-2} & Q_{0,-1} & Q_{0,0} & Q_{0,1} & Q_{0,2} & & \\ & \ddots & \ddots & \ddots & \ddots & \ddots & & \\ & & Q_{N+1,N-1} & Q_{N+1,N} & Q_{N+1,N+1} & Q_{N+1,N+2} & Q_{N+1,N+3} & \\ & & & Q_{N+2,N} & Q_{N+2,N+1} & Q_{N+2,N+2} & Q_{N+2,N+3} & Q_{N+2,N+4} \end{bmatrix},$$
$$W_1 = \begin{bmatrix} w_{i,-3}^{(r)} & w_{i,-2}^{(r)} & \cdots & w_{i,N+3}^{(r)} & w_{i,N+4}^{(r)} \end{bmatrix}^{\mathrm{T}} \tag{6}$$

and

$$\Phi_1 = \left[\frac{\partial^{(r)} Q_{-1}(x_i)}{\partial x^{(r)}} \quad \frac{\partial^{(r)} Q_0(x_i)}{\partial x^{(r)}} \quad \cdots \quad \frac{\partial^{(r)} Q_{N+1}(x_i)}{\partial x^{(r)}} \quad \frac{\partial^{(r)} Q_{N+2}(x_i)}{\partial x^{(r)}} \right]^{\mathrm{T}}. \tag{7}$$

The weighting coefficients $w_{i,j}^{(r)}$ related to the ith grid points are determined by solving system (5). System (5) consists of $N+8$ unknowns and $N+4$ equations. To have a unique solution for the system, it is necessary to eliminate four unknown terms from the equation system. By adding the following equations

$$\frac{\partial^{(r+1)} Q_{-1}(x_i)}{\partial x^{(r+1)}} = \sum_{j=-3}^{1} w_{i,j}^{(r)} Q'_{-1}(x_j), \tag{8}$$

$$\frac{\partial^{(r+1)} Q_0(x_i)}{\partial x^{(r+1)}} = \sum_{j=-2}^{2} w_{i,j}^{(r)} Q'_0(x_j), \tag{9}$$

$$\frac{\partial^{(r+1)} Q_{N+1}(x_i)}{\partial x^{(r+1)}} = \sum_{j=N-1}^{N+3} w_{i,j}^{(r)} Q'_{N+1}(x_j),$$

$$\frac{\partial^{(r+1)} Q_{N+2}(x_i)}{\partial x^{(r+1)}} = \sum_{j=N}^{N+4} w_{i,j}^{(r)} Q'_{N+2}(x_j), \tag{10}$$

to system (5), we easily obtain

$$M_2 W_1 = \Phi_2, \tag{11}$$

where

$$M_2 = \begin{bmatrix}
Q_{-1,-3} & Q_{-1,-2} & Q_{-1,-1} & Q_{-1,0} & Q_{-1,1} & & & \\
Q'_{-1,-3} & Q'_{-1,-2} & Q'_{-1,-1} & Q'_{-1,0} & Q'_{-1,1} & & & \\
 & Q_{0,-2} & Q_{0,-1} & Q_{0,0} & Q_{0,1} & Q_{0,2} & & \\
 & Q'_{0,-2} & Q'_{0,-1} & Q'_{0,0} & Q'_{0,1} & Q'_{0,2} & & \\
 & & Q_{1,-1} & Q_{1,0} & Q_{1,1} & Q_{1,2} & Q_{1,3} & \\
 & & \ddots & \ddots & \ddots & \ddots & \ddots & \\
 & & Q_{N+1,N-1} & Q_{N+1,N} & Q_{N+1,N+1} & Q_{N+1,N+2} & Q_{N+1,N+3} & \\
 & & Q'_{N+1,N-1} & Q'_{N+1,N} & Q'_{N+1,N+1} & Q'_{N+1,N+2} & Q'_{N+1,N+3} & \\
 & & & Q_{N+2,N} & Q_{N+2,N+1} & Q_{N+2,N+2} & Q_{N+2,N+3} & Q_{N+2,N+4} \\
 & & & Q'_{N+2,N} & Q'_{N+2,N+1} & Q'_{N+2,N+2} & Q'_{N+2,N+3} & Q'_{N+2,N+4}
\end{bmatrix}$$

and

$$\Phi_2 = \left[\frac{\partial^{(r)} Q_{-1}(x_i)}{\partial x^{(r)}} \quad \frac{\partial^{(r+1)} Q_{-1}(x_i)}{\partial x^{(r+1)}} \quad \frac{\partial^{(r)} Q_0(x_i)}{\partial x^{(r)}} \quad \frac{\partial^{(r+1)} Q_0(x_i)}{\partial x^{(r+1)}} \quad \frac{\partial^{(r)} Q_1(x_i)}{\partial x^{(r)}} \quad \cdots \quad \frac{\partial^{(r)} Q_{N+1}(x_i)}{\partial x^{(r)}} \quad \frac{\partial^{(r+1)} Q_{N+1}(x_i)}{\partial x^{(r+1)}} \quad \frac{\partial^{(r)} Q_{N+2}(x_i)}{\partial x^{(r)}} \quad \frac{\partial^{(r+1)} Q_{N+2}(x_i)}{\partial x^{(r+1)}} \right]^{\mathrm{T}}.$$

After using values of quintic B-splines at the grid points and eliminating $w_{i,-3}^{(r)}$, $w_{i,-2}^{(r)}$, $w_{i,N+3}^{(r)}$ and $w_{i,N+4}^{(r)}$ from the system, we obtain an algebraic equation system having a five-banded coefficient matrix of the form

$$M_3 W_2 = \Phi_3, \tag{12}$$

where

$$M_3 = \begin{bmatrix}
37 & 82 & 21 & & & & & & \\
8 & 33 & 18 & 1 & & & & & \\
1 & 26 & 66 & 26 & 1 & & & & \\
 & 1 & 26 & 66 & 26 & 1 & & & \\
 & & \ddots & \ddots & \ddots & \ddots & \ddots & & \\
 & & & 1 & 26 & 66 & 26 & 1 & \\
 & & & & 1 & 26 & 66 & 26 & 1 \\
 & & & & & 1 & 18 & 33 & 8 \\
 & & & & & & 21 & 82 & 37
\end{bmatrix}$$

and

$$W_2 = \begin{bmatrix} w_{i,-1}^{(r)} \\ w_{i,0}^{(r)} \\ \vdots \\ w_{i,i-2}^{(r)} \\ w_{i,i-1}^{(r)} \\ w_{i,i}^{(r)} \\ w_{i,i+1}^{(r)} \\ w_{i,i+2}^{(r)} \\ \vdots \\ w_{i,N+1}^{(r)} \\ w_{i,N+2}^{(r)} \end{bmatrix}.$$

The non-zero entries of the load vector Φ_3 are given as

$$\begin{aligned}
\Phi_{-1} &= \frac{1}{30}\Big[-5Q_{-1}^{(r)}(x_i) + hQ_{-1}^{(r+1)}(x_i) \\
&\quad + 40Q_0^{(r)}(x_i) + 8hQ_0^{(r+1)}(x_i)\Big], \\
\Phi_0 &= \frac{1}{10}\Big[5Q_0^{(r)}(x_i) - hQ_0^{(r+1)}(x_i)\Big], \\
\Phi_{i-2} &= Q_{i-2}^{(r)}(x_i), \\
\Phi_{i-1} &= Q_{i-1}^{(r)}(x_i), \\
\Phi_i &= Q_i^{(r)}(x_i), \\
\Phi_{i+1} &= Q_{i+1}^{(r)}(x_i), \\
\Phi_{i+2} &= Q_{i-2}^{(r)}(x_i), \\
\Phi_{N+1} &= \frac{1}{10}\Big[5Q_{N+1}^{(r)}(x_i) + hQ_{N+1}^{(r+1)}(x_i)\Big], \\
\Phi_{N+2} &= \frac{-1}{30}\Big[-40Q_{N+1}^{(r)}(x_i) + 8hQ_{N+1}^{(r+1)}(x_i) \\
&\quad + 5Q_{N+2}^{(r)}(x_i) + hQ_{N+2}^{(r+1)}(x_i)\Big].
\end{aligned} \tag{13}$$

For example, if we apply the test functions Q_m, $m = -1, 0, \ldots, N+2$, at the first grid point x_1 for first-order derivative approximation by the selection of $i = 1$ and $r = 1$ in eq. (13)

$$\begin{aligned}
\Phi_{-1} &= \frac{1}{30}\Big[-5Q_{-1}^{(1)}(x_1) + hQ_{-1}^{(2)}(x_1) \\
&\quad + 40Q_0^{(1)}(x_1) + 8hQ_0^{(2)}(x_1)\Big], \\
\Phi_{-1} &= \frac{1}{30}\left[-5\left(\frac{-5}{h}\right) + h\left(\frac{20}{h^2}\right)\right. \\
&\quad \left. + 40\left(\frac{-50}{h}\right) + 8h\left(\frac{40}{h^2}\right)\right] = \frac{-109}{2h}, \\
\Phi_0 &= \frac{1}{10}\Big[5Q_0^{(1)}(x_1) - hQ_0^{(2)}(x_1)\Big], \\
\Phi_0 &= \frac{1}{10}\left[5\left(\frac{-50}{h}\right) - h\left(\frac{40}{h^2}\right)\right] = \frac{-29}{h}, \\
\Phi_1 &= Q_1^{(1)}(x_1) = 0, \\
\Phi_2 &= Q_2^{(1)}(x_1) = \frac{50}{h}, \\
\Phi_3 &= Q_3^{(1)}(x_1) = \frac{5}{h}, \\
\Phi_{N+1} &= \frac{1}{10}\Big[5Q_{N+1}^{(1)}(x_1) + hQ_{N+1}^{(2)}(x_1)\Big], \\
\Phi_{N+1} &= \frac{1}{10}[5.0 + h.0] = 0, \\
\Phi_{N+2} &= \frac{-1}{30}\Big[-40Q_{N+1}^{(r)}(x_i) + 8hQ_{N+1}^{(r+1)}(x_i) \\
&\quad + 5Q_{N+2}^{(r)}(x_i) + hQ_{N+2}^{(r+1)}(x_i)\Big], \\
\Phi_{N+2} &= \frac{-1}{30}[-40.0 + 8h.0 + 5.0 + h.0] = 0
\end{aligned}$$

is obtained and written in the matrix form as

$$M_3 \begin{bmatrix} w_{1,-1}^{(1)} \\ w_{1,0}^{(1)} \\ w_{1,1}^{(1)} \\ w_{1,2}^{(1)} \\ w_{1,3}^{(1)} \\ w_{1,4}^{(1)} \\ \vdots \\ w_{1,N+1}^{(1)} \\ w_{1,N+2}^{(1)} \end{bmatrix} = \begin{bmatrix} -109/2h \\ -29/h \\ 0 \\ 50/h \\ 5/h \\ 0 \\ \vdots \\ 0 \\ 0 \end{bmatrix}. \tag{14}$$

By following the same idea used before to determine the weighting coefficients $w_{k,j}^{(1)}$, $j = -1, 0, \ldots, N+2$, at grid points x_k, $2 \le k \le N-1$, we have obtained the following algebraic equation system:

$$M_3\begin{bmatrix} w^{(1)}_{k,-1}\\ \vdots\\ w^{(1)}_{k,k-3}\\ w^{(1)}_{k,k-2}\\ w^{(1)}_{k,k-1}\\ w^{(1)}_{k,k}\\ w^{(1)}_{k,k+1}\\ w^{(1)}_{k,k+2}\\ w^{(1)}_{k,k+3}\\ \vdots\\ w^{(1)}_{k,N+2}\end{bmatrix}=\begin{bmatrix}0\\ \vdots\\ 0\\ -5/h\\ -50/h\\ 0\\ 50/h\\ 5/h\\ 0\\ \vdots\\ 0\end{bmatrix}. \tag{15}$$

For the last grid point of the domain x_N with the same idea, we determine the weighting coefficients $w^{(1)}_{N,j}$, $j=-1,0,\ldots,N+2$, and obtain the algebraic equation system as

$$M_3\begin{bmatrix} w^{(1)}_{N,-1}\\ w^{(1)}_{N,0}\\ \vdots\\ w^{(1)}_{N,N-3}\\ w^{(1)}_{N,N-2}\\ w^{(1)}_{N,N-1}\\ w^{(1)}_{N,N}\\ w^{(1)}_{N,N+1}\\ w^{(1)}_{N,N+2}\end{bmatrix}=\begin{bmatrix}0\\ 0\\ \vdots\\ 0\\ -5/h\\ -50/h\\ 0\\ 29/h\\ 109/2h\end{bmatrix}. \tag{16}$$

We can obtain the third-order derivative approximations with similar calculation. Hence, system (12) is solved by the pentadiagonal Thomas algorithm.

3. Numerical discretisation

We have discretised eq. (2) using the forward finite difference and Crank–Nicolson-type schemes. First, eq. (2) is discretised as

$$\frac{U^{n+1}-U^n}{\Delta t}+\mu\frac{U^{n+1}_{3x}+U^n_{3x}}{2} +\varepsilon\frac{\left(U^2U_x\right)^{n+1}+\left(U^2U_x\right)^n}{2}=0. \tag{17}$$

Equation (17) is rewritten as follows:

$$2U^{n+1}+\Delta t\Big[\mu U^{n+1}_{3x}+\varepsilon\big(U^2U_x\big)^{n+1}\Big] =2U^n+\Delta t\Big[-\mu U^n_{3x}-\varepsilon\big(U^2U_x\big)^n\Big]. \tag{18}$$

Then, the Rubin and Graves-type linearisation technique [45] is used on the left-hand side of eq. (18) to linearise the nonlinear terms as given below:

$$(UU_x)^{n+1}=\left(U^{n+1}U^n_x+U^nU^{n+1}_x-U^nU^n_x\right), \tag{19}$$
$$(UU_x)^n=U^nU^n_x. \tag{20}$$

Accordingly, we have obtained

$$2U^{n+1}+\Delta t\Big[\mu U^{n+1}_{3x}+\varepsilon\Big(\big(U^2\big)^nU^{n+1}_x+2U^nU^n_xU^{n+1}\Big)\Big] =2U^n+\Delta t\Big[-\mu U^n_{3x}+\varepsilon\big(U^2\big)^nU^n_x\Big]. \tag{21}$$

Let us define some terms used in eq. (21) as

$$A^n_i=\sum_{j=1}^{N}w^{(1)}_{ij}U^n_j=U^n_{x_i},$$
$$B^n_i=\sum_{j=1}^{N}w^{(3)}_{ij}U^n_j=U^n_{3x_i}, \tag{22}$$

where A^n_i and B^n_i are the first- and third-order derivative approximations of the U functions at the nth time level on points x_i, respectively. By substituting definition (22) in eq. (21), we obtain

$$2U^{n+1}_i+\Delta t\left[\mu\sum_{j=1}^{N}w^{(3)}_{ij}U^{n+1}_j +\varepsilon\left(\left(U^n_i\right)^2\sum_{j=1}^{N}w^{(1)}_{ij}U^{n+1}_j+2U^n_iA^n_iU^{n+1}_i\right)\right] =\phi^n_i, \tag{23}$$

where

$$\phi^n_i=2U^n_i+\Delta t\Big[-\mu B^n_i+\varepsilon\big(U^n_i\big)^2A^n_i\Big],$$

for $i=1(1)N$.

Then we have reorganised eq. (23) for each grid point as follows:

$$\Big[2+\Delta t\Big(\mu w^{(3)}_{ii}+\varepsilon\Big(\big(U^n_i\big)^2w^{(1)}_{ii}+2U^n_iA^n_i\Big)\Big)\Big]U^{n+1}_i +\left[\sum_{j=1,i\neq j}^{N}\Delta t\Big(\mu w^{(3)}_{ij}+\varepsilon\left(U^n_i\right)^2w^{(1)}_{ij}\Big)U^{n+1}_j\right] =\phi^n_i. \tag{24}$$

By implementing the system of eq. (24) on x_i, $i = 1(1)N$ grid points, N equations consisting of N unknowns which are denoted by U^{n+1} will be obtained. The equation system is shown in the matrix form below:

$$\begin{bmatrix} K_{1,1} & K_{1,2} & \cdots & K_{1,N} \\ K_{2,1} & K_{2,2} & \cdots & K_{2,N} \\ \vdots & \vdots & \ddots & \vdots \\ K_{N-1,1} & K_{N-1,2} & \cdots & K_{N-1,N} \\ K_{N,1} & K_{N,2} & \cdots & K_{N,N} \end{bmatrix} \begin{bmatrix} U_1^{n+1} \\ U_2^{n+1} \\ \vdots \\ U_{N-1}^{n+1} \\ U_N^{n+1} \end{bmatrix} = \begin{bmatrix} \phi_1^n \\ \phi_2^n \\ \vdots \\ \phi_{N-1}^n \\ \phi_N^n \end{bmatrix}. \tag{25}$$

Then the boundary conditions are applied to the system of eq. (25) and the first and last equations are eliminated from the systems. Hence,

$$\begin{bmatrix} K_{2,2} & K_{2,3} & \cdots & K_{2,N-1} \\ K_{3,2} & K_{3,3} & \cdots & K_{3,N-1} \\ \vdots & \vdots & \ddots & \vdots \\ K_{N-1,2} & K_{N-1,3} & \cdots & K_{N-1,N-1} \end{bmatrix} \begin{bmatrix} U_2^{n+1} \\ U_3^{n+1} \\ \vdots \\ U_{N-1}^{n+1} \end{bmatrix} = \begin{bmatrix} \phi_2^n - K_{2,1}U_1^{n+1} - K_{2,N}U_N^{n+1} \\ \phi_3^n - K_{3,1}U_1^{n+1} - K_{3,N}U_N^{n+1} \\ \vdots \\ \phi_{N-1}^n - K_{N-1,1}U_1^{n+1} - K_{N-1,N}U_N^{n+1} \end{bmatrix} \tag{26}$$

is obtained and solved by the Gauss elimination method easily.

4. Numerical examples

In this section, the five well-known test problems are investigated. The accuracy of the numerical method is checked by using the error norms L_2 and L_∞, respectively:

$$L_2 = \sqrt{h \sum_{J=1}^{N} \left| U_j^{\text{exact}} - (U_N)_j \right|^2},$$
$$L_\infty = \max_j \left| U_j^{\text{exact}} - (U_N)_j \right|. \tag{27}$$

Moreover, the following lowest three invariants corresponding to the conservation of mass, momentum and energy are computed:

$$I_1 = \int_a^b U\,\mathrm{d}x, \quad I_2 = \int_a^b U^2\mathrm{d}x,$$
$$I_3 = \int_a^b \left[U^4 - \frac{6\mu}{\varepsilon} \left(U'\right)^2 \right] \mathrm{d}x. \tag{28}$$

4.1 *Single soliton*

The mKdV equation has an analytic solution given in the following form:

$$U(x,t) = kp\,\mathrm{sech}\big(kx - kx_0 - k^3\mu t\big), \tag{29}$$

where

$$p = \left[\frac{6\mu}{\varepsilon}\right]^{1/2}, \tag{30}$$

which represents a single soliton originally located at x_0 moving to the right with velocity $k^2\mu$. Solitons may have positive or negative amplitudes depending on the sign of k but all of them have positive velocities. We take eq. (29) as initial condition at $t = 0$ of the form

$$U(x,0) = kp\,\mathrm{sech}(kx - kx_0), \tag{31}$$

and to allow comparison with earlier works [29,30], we use $\varepsilon = 3$, $\mu = 1$, $kp = c = 1.3$, $x_0 = 15$ and $0 \le x \le 200$. For the present case, the obtained solution is going to move towards the right, having a constant speed with unchanged amplitude. We have plotted the graphs of the numerical solution of a single soliton with $\Delta t = 0.025$ and $N = 1001$ from $t = 0$ to 100 in figure 1. To make a quantitative comparison, the error norms L_2 and L_∞ have been computed and compared with earlier works [29,30] in table 1 until $t = 10$, respectively. It is clearly seen from table 1 that by using the same parameters ($\Delta t = 0.025$) and less number of grid points ($N = 761$), the present results are superior. Besides this, by decreasing the time step size from $\Delta t = 0.025$ to 0.001, the error norms L_2 and L_∞ decrease to 1.6×10^{-5} and 1.0×10^{-5}, respectively at $t = 10$. After that, three lowest invariants, I_1, I_2 and I_3, are computed with the same parameters $\Delta t = 0.025$ and $N = 1001$ and compared with earlier works [29,30] in table 2 until $t = 100$. It is seen from table 2 that the present results are superior, again. It is obviously seen from table 2 that the three lowest invariants, I_1, I_2 and I_3, are changed by less than 2.7×10^{-6}, -4.4×10^{-5} and -1.3×10^{-4}, respectively, with respect to their original values during the long run $t = 100$ and so are small enough to accept. To show the accuracy of the present method for a long time, i.e. $t = 100$ with a small time

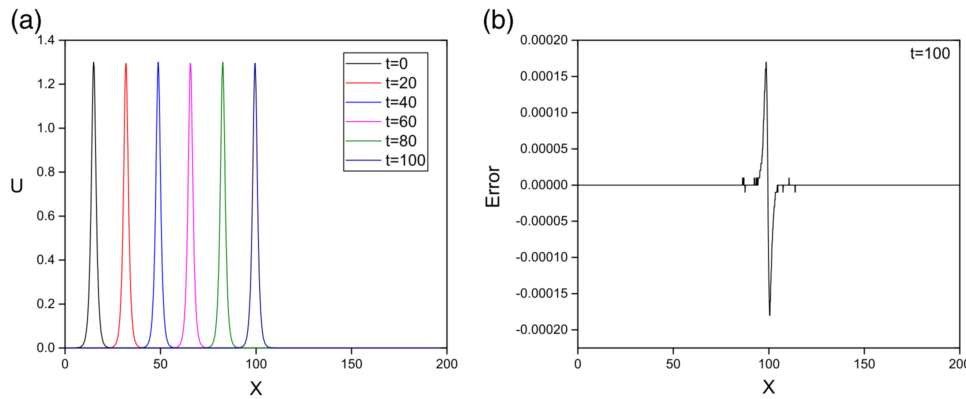

Figure 1. (**a**) Simulations of a single soliton and (**b**) maximum error at $t = 100$.

Table 1. The error norms L_2 and L_∞ at various times for a single soliton.

	QCN-DQM (present)						$\Delta t = 0.025$ and $N = 1000$			
	$\Delta t = 0.025$, $N = 761$		$\Delta t = 0.01$, $N = 1201$		$\Delta t = 0.001$, $N = 2001$		Quad. FEM [29]		Quin. FEM [30]	
t	$L_2 \times 10^3$	$L_\infty \times 10^3$	$L_2 \times 10^3$	$L_\infty \times 10^3$	$L_2 \times 10^3$	$L_\infty \times 10^3$	$L_2 \times 10^3$	$L_\infty \times 10^3$	$L_2 \times 10^3$	$L_\infty \times 10^3$
0	–	–	–	–	–	–	–	–	–	–
1	0.321	0.172	0.048	0.032	0.008	0.004	3.38	2.03	0.25	0.10
2	0.322	0.202	0.051	0.030	0.008	0.005	4.88	3.23	0.35	0.17
3	0.322	0.195	0.049	0.031	0.009	0.005	6.32	4.15	0.39	0.25
4	0.289	0.206	0.045	0.032	0.009	0.006	7.65	5.00	0.51	0.36
5	0.311	0.220	0.049	0.035	0.011	0.007	8.84	5.75	0.75	0.51
6	0.318	0.203	0.049	0.033	0.012	0.008	9.83	6.34	1.02	0.67
7	0.307	0.211	0.049	0.035	0.013	0.008	10.57	6.71	1.32	0.85
8	0.300	0.192	0.048	0.033	0.013	0.008	11.21	7.20	1.66	1.07
9	0.315	0.214	0.048	0.032	0.015	0.010	11.34	6.99	2.03	1.03
10	0.313	0.207	0.050	0.034	0.016	0.010	11.61	7.33	2.45	1.55

Table 2. Comparison of the three lowest invariants for a single soliton: $\Delta t = 0.025$, $N = 1001$.

	QCN-DQM (present)			Quad. FEM [29]			Quin. FEM [30]		
t	I_1	I_2	I_3	I_1	I_2	I_3	I_1	I_2	I_3
0	4.442880	3.676954	2.071352	4.443	3.678	2.055	4.443	3.677	2.071
10	4.442868	3.676935	2.071318	4.444	3.677	2.055	4.442	3.676	2.070
20	4.442869	3.676923	2.071299	4.443	3.677	2.054	4.442	3.675	2.068
30	4.442881	3.676905	2.071267	4.444	3.676	2.054	4.442	3.674	2.067
40	4.442893	3.676892	2.071248	4.444	3.676	2.054	4.441	3.674	2.066
50	4.442897	3.676876	2.071218	4.443	3.676	2.054	4.441	3.673	2.064
60	4.442883	3.676856	2.071186	4.442	3.676	2.053	4.440	3.672	2.063
70	4.442893	3.676846	2.071167	4.441	3.676	2.053	4.440	3.671	2.061
80	4.442887	3.676825	2.071132	4.441	3.676	2.053	4.440	3.670	2.060
90	4.442888	3.676816	2.071119	4.440	3.675	2.052	4.439	3.669	2.058
100	4.442892	3.676794	2.071082	4.440	3.675	2.052	4.439	3.668	2.057

step size $\Delta t = 0.001$, three lowest invariants I_1, I_2 and I_3 and error norms L_2 and L_∞ are computed and are given in table 3. It is clearly seen from table 3 that the present method gives acceptable good results for a long simulation and at time $t = 100$ the three invariants I_1, I_2 and I_3 are changed by less than 1.2×10^{-6}, -3.8×10^{-6}

Table 3. The three lowest invariants and error norms for a single soliton: $\Delta t = 0.001$, $N = 2001$.

	QCN-DQM (present)				
t	I_1	I_2	I_3	$L_2 \times 10^3$	$L_\infty \times 10^3$
0	4.442877	3.676955	2.071352	–	–
10	4.442882	3.676955	2.071352	0.016	0.010
20	4.442876	3.676947	2.071340	0.017	0.011
30	4.442880	3.676941	2.071328	0.024	0.016
40	4.442874	3.676935	2.071317	0.083	0.053
50	4.442875	3.676934	2.071317	0.153	0.094
60	4.442877	3.676940	2.071325	0.205	0.123
70	4.442880	3.676934	2.071317	0.259	0.155
80	4.442880	3.676944	2.071331	0.309	0.185
90	4.442881	3.676938	2.071325	0.352	0.207
100	4.442882	3.676941	2.071327	0.403	0.239

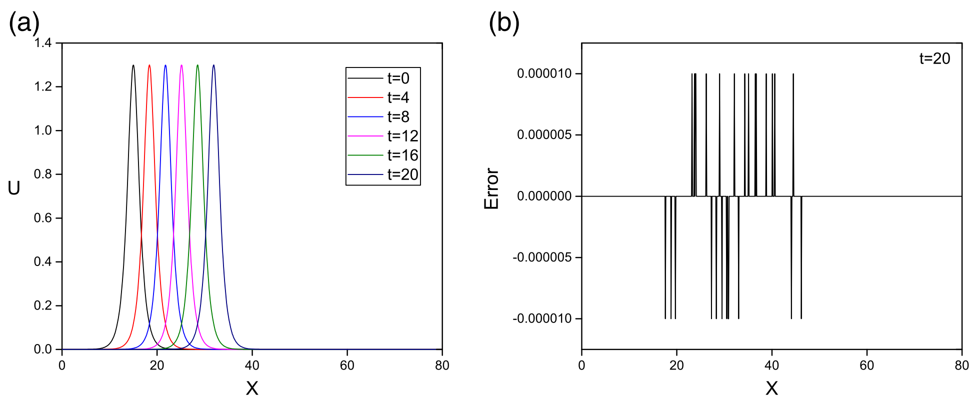

Figure 2. (**a**) Simulations of a single soliton and (**b**) maximum error at $t = 20$.

and -1.2×10^{-5}, respectively, with respect to their original values during this very long run and therefore they can be considered almost constant. The maximum error value of a single soliton at $t = 100$ for the simulation region $0 \le x \le 200$ is given in figure 1.

Then to compare with other works [26–28] we fix all parameters except solution region $0 \le x \le 80$ and time $0 \le t \le 20$. We have plotted the graphs of the numerical solution of single soliton with $\Delta t = 0.01$ and $N = 475$ from $t = 0$ to 20 in figure 2. To make a quantitative comparison, the error norms L_2 and L_∞ and three lowest invariants I_1, I_2 and I_3 have been computed and compared with earlier works [26–28] in table 4 till $t = 20$. It is clearly seen from table 4 that by using the same parameters ($\Delta t = 0.01$) and less number of grid points ($N = 475$) than earlier works [26–28], the present results are superior and the error norms L_2 and L_∞ are obtained as 5.0×10^{-5} and 3.1×10^{-5} respectively at $t = 20$. Besides these, by decreasing the time step size from $\Delta t = 0.01$ to 0.001, the error norms L_2 and L_∞ decrease to 9.9×10^{-6} and 6.2×10^{-6} respectively at $t = 20$. The maximum error value of a single soliton at $t = 20$ for the simulation region $0 \le x \le 80$ is given in figure 2.

4.2 *Interaction of double solitons*

The interaction of double solitons has an initial condition of the form [29,30]

$$U(x,t) = \sum_{i=1}^{2} k_i p \operatorname{sech}\left(k_i x - k_i x_i - k_i^3 \mu t\right), \tag{32}$$

where

$$p = \left[\frac{6\mu}{\varepsilon}\right]^{1/2}, \tag{33}$$

evaluated at $t = 0$.

This condition represents two solitary waves moving to the right having velocities $k_i^2\mu$ which depend

Table 4. The three lowest invariants and L_2 and L_∞ error norms for a single soliton.

Method	t	$L_2 \times 10^3$	$L_\infty \times 10^3$	I_1	I_2	I_3
Present QCN-DQM	0	–	–	4.442881	3.676955	2.071352
$\Delta t = 0.01$, $N = 475$	1	0.048278	0.029429	4.442885	3.676954	2.071352
	5	0.049183	0.031314	4.442894	3.676955	2.071353
	10	0.052029	0.034742	4.442872	3.676954	2.071350
	15	0.051401	0.037722	4.442872	3.676953	2.071347
	20	0.050776	0.031535	4.442873	3.676950	2.071343
Present QCN-DQM	0	–	–	4.442877	3.676955	2.071352
$\Delta t = 0.001$, $N = 801$	1	0.007319	0.003647	4.442881	3.676954	2.071351
	5	0.010969	0.007443	4.442880	3.676949	2.071342
	10	0.012061	0.008346	4.442877	3.676949	2.071342
	15	0.011568	0.009028	4.442876	3.676946	2.071337
	20	0.009997	0.006212	4.442879	3.676950	2.071345
Gal. FEM [26]	0	–	–	–	–	–
$\Delta t = 0.01$, $N = 801$	1	–	1.206756	4.443000	3.677069	2.073575
	5	–	3.621519	4.443138	3.677535	2.074357
	10	–	5.942047	4.444142	3.678094	2.075303
	15	–	7.626772	4.443420	3.678642	2.076232
	20	–	8.642137	4.443171	3.679192	2.077161
Lump. Pet-Gal.FEM [27]	0	–	–	–	–	–
$\Delta t = 0.01$, $N = 801$	1	0.628695	0.363099	4.442866	3.676941	2.072795
	5	1.249516	0.839746	4.442866	3.676941	2.073537
	10	2.131860	1.399503	4.442866	3.676941	2.073699
	15	2.949376	1.880855	4.442866	3.676941	2.073776
	20	3.641638	2.285638	4.442866	3.676941	2.073846
Lump-Gal. FEM [28]	0	–	–	–	–	–
$\Delta t = 0.01$, $N = 801$	1	0.627901	0.362434	4.442866	3.676941	2.072792
	5	1.252048	0.841523	4.442866	3.676941	2.073533
	10	2.138787	1.403498	4.442866	3.676941	2.073695
	15	2.960441	1.887116	4.442866	3.676941	2.073772
	20	3.656694	2.294197	4.442866	3.676941	2.073841

upon their magnitude. To provide the interaction with increasing time, we place the larger soliton to the left side of the smaller one. Thus, we place the soliton with magnitude $k_1 p = c_1 = 1.3$ at $x_1 = 15$ and $k_2 p = c_2 = 0.9$ at $x_2 = 35$ and then the region is $0 \le x \le 200$, $\varepsilon = 3$, $\mu = 1.0$ so that $p = \sqrt{2}$.

For simulation of interaction of double solitons, we used $\Delta t = 0.025$ and $N = 901$ for a long run from time $t = 0$ to 120. As can be seen in figure 3, the bigger soliton at the left position of the smaller soliton is located at the beginning of the run. With the increase of time, the bigger soliton catches up with the smaller one until $t = 40$, and the smaller soliton is being absorbed. The overlapping process continues until $t = 60$, then the bigger soliton overtakes the smaller soliton and starts the process of separation. At $t = 100$, the interaction is complete and the bigger soliton separates completely from the smaller soliton. Three lowest invariants are calculated and compared with earlier works [29,30] in table 5. By using the same parameter ($\Delta t = 0.025$) and less number of grid points ($N = 901$) than earlier works [29,30], the three invariants I_1, I_2 and I_3 change by less than 6.4×10^{-6}, -1.7×10^{-5} and -6.6×10^{-5}, respectively, at the end of the simulation with respect to their original values during the very long run and therefore they can be considered to be almost constant. We have decreased the time step size from $\Delta t = 0.025$ to 0.01 and used less number of grid points ($N = 871$), then I_2 invariants do not change and I_1 and I_3 invariants change by less than 8.9×10^{-6} and 3.6×10^{-7}, respectively, at the end of the simulation with respect to their original values.

Then, to compare with another work [26] we used

$$U(x,0) = \sum_{i=1}^{2} \alpha_i \operatorname{sech}\left[\sqrt{\frac{c_i}{\mu}}\,(x - x_i)\right] \tag{34}$$

as initial condition where

$$\alpha_i = \left[\frac{6c_i}{\varepsilon}\right]^{1/2}, \quad i = 1, 2 \tag{35}$$

and $\varepsilon = 3$, $\mu = 1$, $c_1 = 2$, $c_2 = 1$, $x_1 = 15$ and $x_2 = 25$ at solution region $0 \le x \le 80$ and time $0 \le t \le 20$. We have plotted the graphs of the numerical solution of

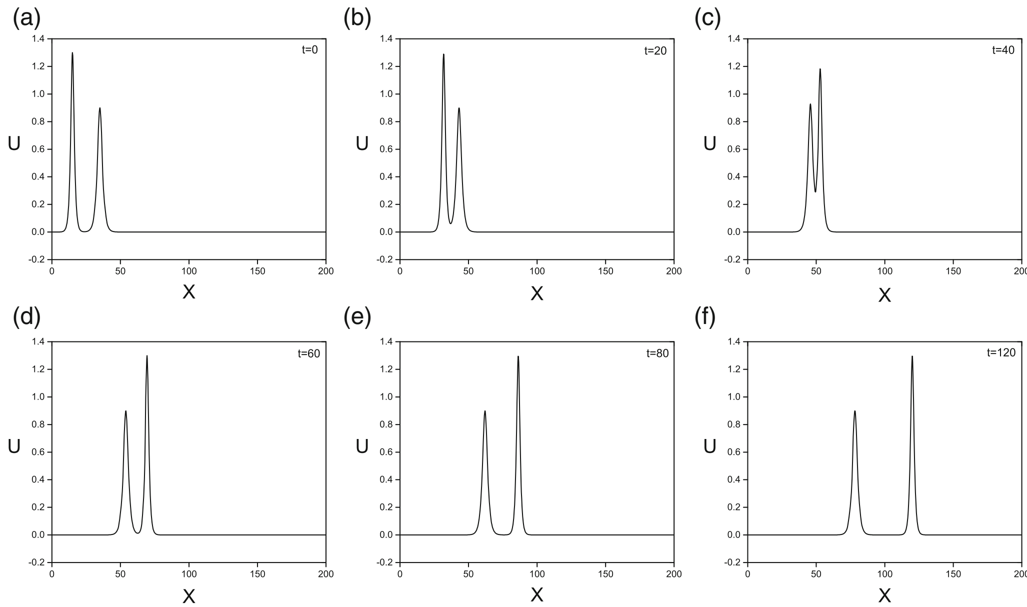

Figure 3. Simulations of double solitons: (**a**) $t = 0$, (**b**) $t = 20$, (**c**) $t = 40$, (**d**) $t = 60$, (**e**) $t = 80$ and (**f**) $t = 120$.

Table 5. Invariants for double solitons: $c_1 = 1.3$ and $c_2 = 0.9$.

t	I_1	I_2	I_3	I_1	I_2	I_3
	$\Delta t = 0.025$ and $N = 901$ QCN-DQM (present)			$\Delta t = 0.01$ and $N = 871$ QCN-DQM (present)		
0	8.885761	6.222641	2.758834	8.885756	6.222640	2.758833
20	8.885755	6.222616	2.758789	8.885740	6.222646	2.758843
40	8.885790	6.222559	2.758680	8.885780	6.222632	2.758847
60	8.885807	6.222596	2.758753	8.885852	6.222641	2.758835
80	8.885818	6.222576	2.758721	8.885843	6.222637	2.758826
100	8.885799	6.222555	2.758684	8.885837	6.222641	2.758836
120	8.885818	6.222536	2.758651	8.885835	6.222640	2.758834
	$\Delta t = 0.025$ and $N = 1000$ Quad. FEM [29]			$\Delta t = 0.025$ and $N = 1000$ Quin. FEM [30]		
0	8.8857	6.2226	2.7396	8.8858	6.2226	2.7588
20	8.8865	6.2222	2.7389	8.8852	6.2212	2.7562
40	8.8846	6.2220	2.7388	8.8854	6.2212	2.7559
60	8.8845	6.2248	2.7486	8.8851	6.2203	2.7540
80	8.8851	6.2253	2.7495	8.8846	6.2188	2.7513
100	8.8854	6.2219	2.7383	8.8840	6.2174	2.7487
120	8.8846	6.2211	2.7362	8.8834	6.2161	2.7461

double solitons with $\Delta t = 0.01$ and $N = 801$ from $t = 0$ to 20, in figure 4. To make a quantitative comparison, all parameters which were used in the earlier work [26] are used here and the three lowest invariants I_1, I_2 and I_3 have been computed and compared with earlier work [26] in table 6 until $t = 20$. As can be clearly seen from table 6, by using the same parameters as in earlier work [26], the present results are superior. Besides these, by decreasing the time step size from $\Delta t = 0.01$ to 0.001 with less number of grid points ($N = 601$) than earlier work [26], the relative changes of invariants I_1, I_2 and I_3 decrease to -6.5×10^{-6}, 9.3×10^{-7} and 9.8×10^{-7} at $t = 20$, respectively.

4.3 *Interaction of triple solitons*

The interaction of triple solitons has initial condition of the form [26]

$$U(x, 0) = \sum_{i=1}^{3} \alpha_i \operatorname{sech}\left[\sqrt{\frac{c_i}{\mu}}\,(x - x_i)\right], \tag{36}$$

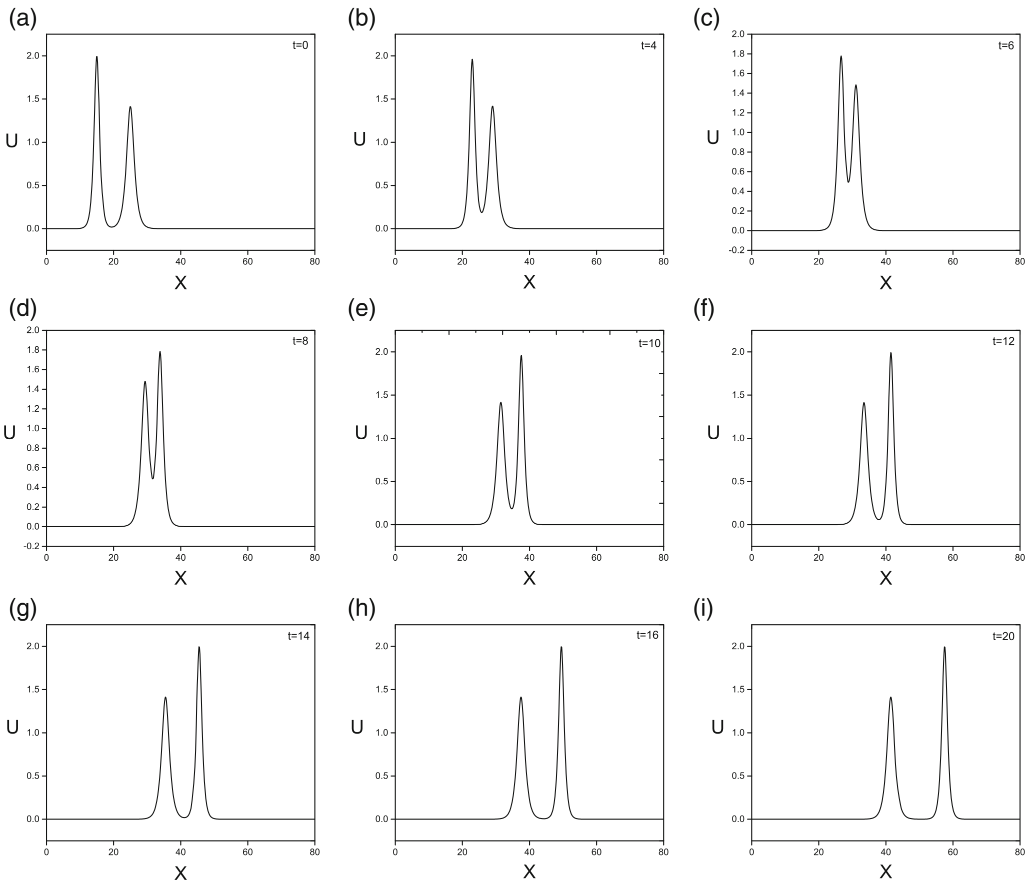

Figure 4. Simulations of double solitons: (**a**) $t = 0$, (**b**) $t = 4$, (**c**) $t = 6$, (**d**) $t = 8$, (**e**) $t = 10$, (**f**) $t = 12$, (**g**) $t = 14$, (**h**) $t = 16$ and (**i**) $t = 20$.

Table 6. Invariants for double solitons: $c_1 = 2$ and $c_2 = 1$.

	$\Delta t = 0.01$ and $N = 801$ QCN-DQM (present)			$\Delta t = 0.001$ and $N = 601$ QCN-DQM (present)			$\Delta t = 0.01$ and $N = 800$ Gal. FEM [26]		
t	I_1	I_2	I_3	I_1	I_2	I_3	I_1	I_2	I_3
0	8.885763	9.659376	10.219340	8.885761	9.659375	10.219340	–	–	–
1	8.885799	9.659359	10.219250	8.885782	9.659382	10.219350	8.886014	9.659527	10.239870
5	8.885741	9.659147	10.218240	8.885767	9.659382	10.219400	8.886776	9.663714	10.249000
10	8.885828	9.659196	10.218550	8.885808	9.659379	10.219360	8.889742	9.662547	10.246790
15	8.885797	9.659162	10.218510	8.885737	9.659385	10.219360	8.885983	9.661071	10.242580
20	8.885759	9.659080	10.218200	8.885703	9.659384	10.219350	8.884880	9.661224	10.242030

where

$$\alpha_i = \left[\frac{6c_i}{\varepsilon}\right]^{1/2}, \quad i = 1, 2, 3 \tag{37}$$

and $\varepsilon = 3$, $\mu = 1$, $c_1 = 2$, $c_2 = 1$, $c_3 = 0.5$, $x_1 = 15$, $x_2 = 25$ and $x_3 = 35$ at the solution region $0 \leq x \leq 80$ and time $0 \leq t \leq 20$. We have plotted the graphs of the numerical solution of triple solitons with $\Delta t = 0.01$ and $N = 301$ from $t = 0$ to 20 in figure 5. To make a quantitative comparison, all parameters which were used in the earlier work [26] are used here also and the three lowest invariants I_1, I_2 and I_3 have been computed and compared with the earlier work [26] in table 7 until $t = 20$. It is seen clearly from table 7 that by using same parameters ($\Delta t = 0.01$) and less number of grid points ($N = 301$) than earlier work [26], the present

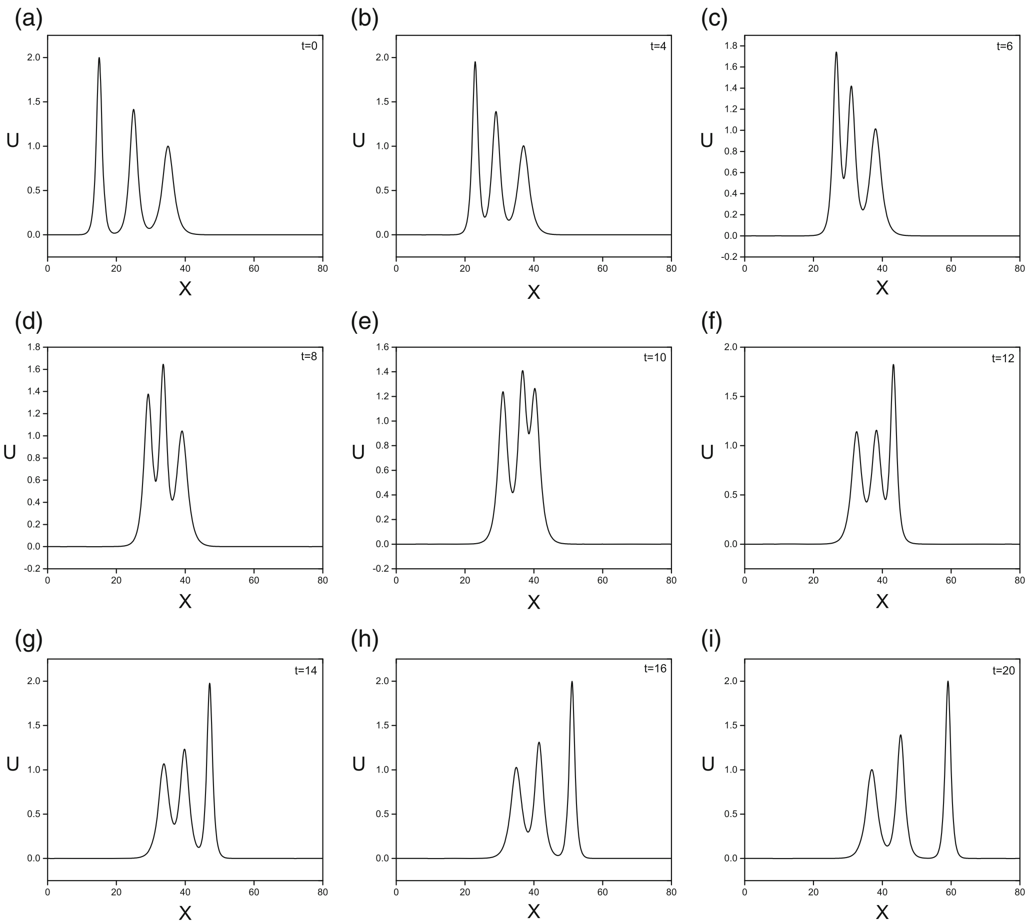

Figure 5. Simulations of triple solitons: (**a**) $t = 0$, (**b**) $t = 4$, (**c**) $t = 6$, (**d**) $t = 8$, (**e**) $t = 10$, (**f**) $t = 12$, (**g**) $t = 14$, (**h**) $t = 16$ and (**i**) $t = 20$.

results are superior. The relative changes of invariants I_1, I_2 and I_3 obtained are, -4.5×10^{-5}, -4.8×10^{-6} and -4.9×10^{-5} respectively at time $t = 20$. Besides these, by decreasing the time step size from $\Delta t = 0.01$ to 0.001 and less number of grid points ($N = 361$) than earlier work [26], the relative changes of invariants I_1, I_2 and I_3 decrease to 2.1×10^{-5}, 0.0×10^{-7} and 8.9×10^{-7}, respectively at time $t = 20$.

4.4 *Maxwellian initial condition*

Evolution of the train of solitons of the mKdV equation has been studied using the Maxwellian initial condition

$$U(x, 0) = \exp\left(-x^2\right) \tag{38}$$

for various values of μ. First of all, to compare the present results with earlier studies, we have selected the

Table 7. Invariants for three solitons: $c_1 = 2$, $c_2 = 1$ and $c_3 = 0.5$.

	$\Delta t = 0.01$ and $N = 301$ QCN-DQM (present)			$\Delta t = 0.001$ and $N = 361$ QCN-DQM (present)			$\Delta t = 0.01$ and $N = 800$ Gal. FEM [26]		
t	I_1	I_2	I_3	I_1	I_2	I_3	I_1	I_2	I_3
0	13.328650	12.519940	11.228820	13.328650	12.519940	11.228610	–	–	–
1	13.328750	12.519920	11.228720	13.328640	12.519940	11.228620	13.329060	12.520280	11.249790
5	13.328650	12.519750	11.228660	13.328450	12.519930	11.229070	13.330630	12.526260	11.261270
10	13.328530	12.519490	11.228930	13.328540	12.519930	11.229800	13.338780	12.540860	11.288040
15	13.327100	12.519830	11.228480	13.327750	12.519940	11.228700	13.332640	12.526660	11.259970
20	13.328050	12.519880	11.228260	13.328920	12.519940	11.228620	13.332060	12.524900	11.256730

Table 8. Invariants for Maxwellian initial condition: $\mu = 0.04$, $\mu = 0.01$, $\mu = 0.005$ and $\mu = 0.0025$.

t	I_1	I_2	I_3	I_1	I_2	I_3	I_1	I_2	I_3	I_1	I_2	I_3
	QCN-DQM $\mu = 0.04$ $\Delta t = 0.01$, $N = 1001$			[29] $\mu = 0.04$ $\Delta t = 0.01$, $N = 1000$			QCN-DQM $\mu = 0.01$ $\Delta t = 0.005$, $N = 751$			[29] $\mu = 0.01$ $\Delta t = 0.005$, $N = 2000$		
0.0	1.7725	1.2533	0.5854	1.7725	1.2533	0.5839	1.7725	1.2533	0.8110	1.7725	1.2533	0.8109
2.5	1.7725	1.2533	0.5854	1.7719	1.2511	0.5756	1.7725	1.2533	0.8110	1.7713	1.2485	0.7889
5.0	1.7725	1.2533	0.5854	1.7716	1.2504	0.5734	1.7725	1.2533	0.8110	1.7708	1.2463	0.7778
7.5	1.7725	1.2533	0.5854	1.7716	1.2501	0.5726	1.7724	1.2533	0.8110	1.7707	1.2460	0.7767
10.0	1.7725	1.2533	0.5854	1.7715	1.2501	0.5723	1.7725	1.2533	0.8110	1.7706	1.2459	0.7764
12.5	1.7725	1.2533	0.5854	1.7716	1.2500	0.5721	1.7725	1.2533	0.8110	1.7706	1.2458	0.7762
	QCN-DQM $\mu = 0.005$ $\Delta t = 0.005$, $N = 1001$			[29] $\mu = 0.005$ $\Delta t = 0.005$, $N = 3000$			QCN-DQM $\mu = 0.0025$ $\Delta t = 0.005$, $N = 1101$			[29] $\mu = 0.0025$ $\Delta t = 0.005$, $N = 3000$		
0.0	1.7725	1.2533	0.8486	1.7725	1.2533	0.8486	1.7725	1.2533	0.8674	1.7725	1.2533	0.8674
2.5	1.7725	1.2533	0.8487	1.7724	1.2529	0.8464	1.7725	1.2534	0.8675	1.7722	1.2520	0.8614
5.0	1.7725	1.2533	0.8486	1.7722	1.2522	0.8438	1.7724	1.2534	0.8674	1.7710	1.2488	0.8504
7.5	1.7725	1.2533	0.8486	1.7720	1.2516	0.8418	1.7725	1.2534	0.8674	1.7699	1.2458	0.8410
10.0	1.7725	1.2533	0.8486	1.7719	1.2510	0.8399	1.7725	1.2535	0.8674	1.7689	1.2431	0.8325
12.5	1.7724	1.2533	0.8486	1.7717	1.2504	0.8380	1.7725	1.2535	0.8675	1.7680	1.2406	0.8247

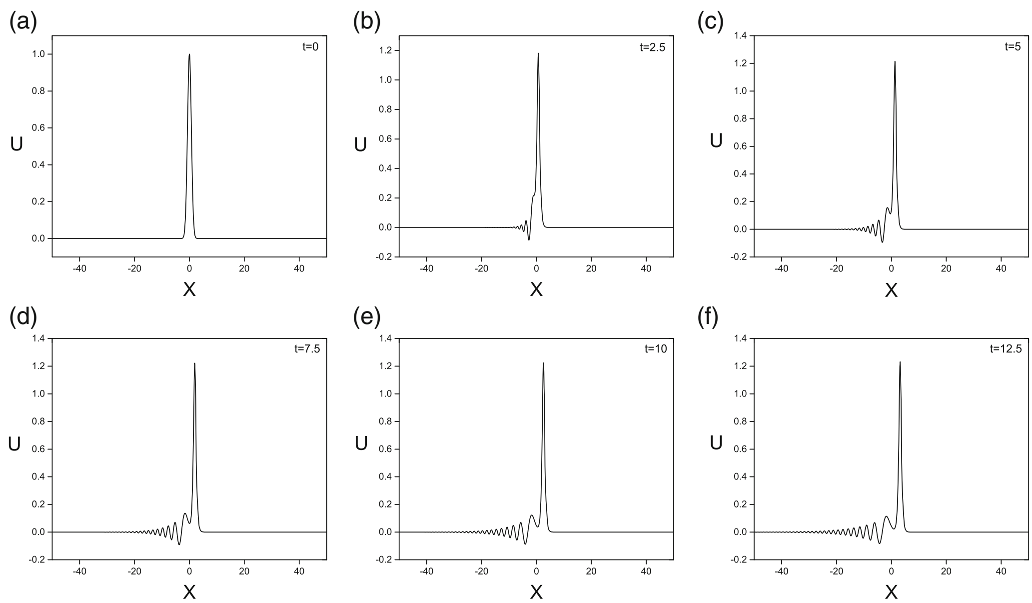

Figure 6. Simulations of Maxwellian initial condition for $\mu = 0.04$: (**a**) $t = 0$, (**b**) $t = 2.5$, (**c**) $t = 5$, (**d**) $t = 7.5$, (**e**) $t = 10$ and (**f**) $t = 12.5$.

values $\varepsilon = 1$, $\mu = 0.04$, $\Delta t = 0.01$ and $N = 1001$ over the region $-50 \leq x \leq 50$. Then, we have used $\mu = 0.01$, $\Delta t = 0.005$ and $N = 751$ over the region $-15 \leq x \leq 15$. Finally, for $\mu = 0.005$ and 0.0025 the simulations are obtained for $\Delta t = 0.005$ and $N = 1001$ and 1101, respectively. The three lowest invariants for all the values of μ are calculated and compared with the earlier work [29] in table 8. One can see clearly from table 8 that the present method used the same parameters and less number of grid points than the earlier work [29] and obtained better results. The graphs drawn using the values $\mu = 0.04$, 0.01, 0.005 and 0.0025 at various times up to $t = 12.5$ are given in figures 6–9. One can see clearly from figures 6–9 that by the decreasing the value of μ from $\mu = 0.04$ to 0.0025, the number of waves increase at the end of the simulations.

4.5 *Tanh initial condition*

Finally, we have examined the tanh initial condition [29]

$$U(x, 0) = 0.5\left[1 - \tanh\frac{|x| - x_0}{d}\right]$$

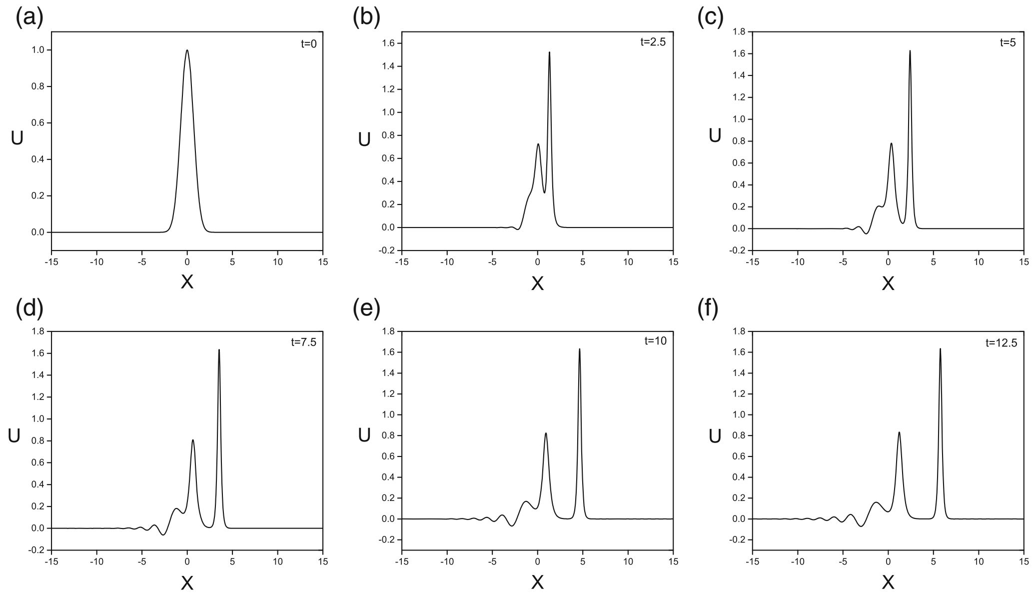

Figure 7. Simulations of Maxwellian initial condition for $\mu = 0.01$: (**a**) $t = 0$, (**b**) $t = 2.5$, (**c**) $t = 5$, (**d**) $t = 7.5$, (**e**) $t = 10$ and (**f**) $t = 12.5$.

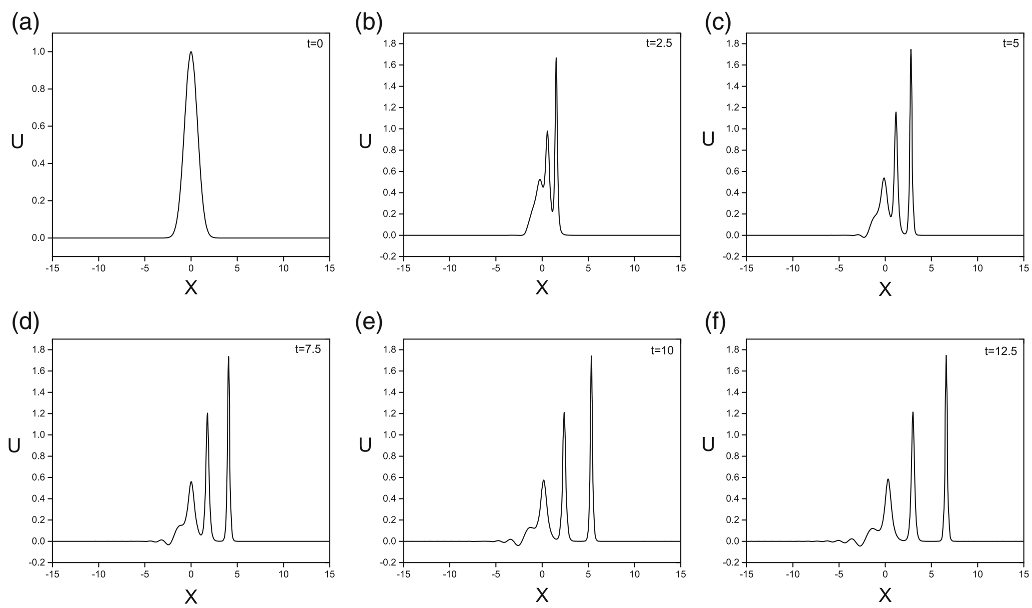

Figure 8. Simulations of Maxwellian initial condition for $\mu = 0.005$: (**a**) $t = 0$, (**b**) $t = 2.5$, (**c**) $t = 5$, (**d**) $t = 7.5$, (**e**) $t = 10$ and (**f**) $t = 12.5$.

and boundary conditions

$$U(-150, t) = U(150, t) = 0, \quad t > 0,$$

where $-150 \le x \le 150$, $d = 5$ and $x_0 = 25$ will be considered in all simulations.

We have taken the same parameters as in [29], i.e., $\varepsilon = 0.2$, $\mu = 0.1$, $\Delta t = 0.05$ and $N = 801$. The behaviour of this simulation that runs for a long time from $t = 0$ to 800 is given in figure 10. The three lowest invariants I_1, I_2 and I_3 are recorded and compared with [29] in table 9 for the present case. It is seen from table 9 that the invariants change by less than 1.2×10^{-5}, 1.5×10^{-4} and 1.1×10^{-5}, respectively, with respect to their original values during this very long run and therefore they can be considered to be almost constant.

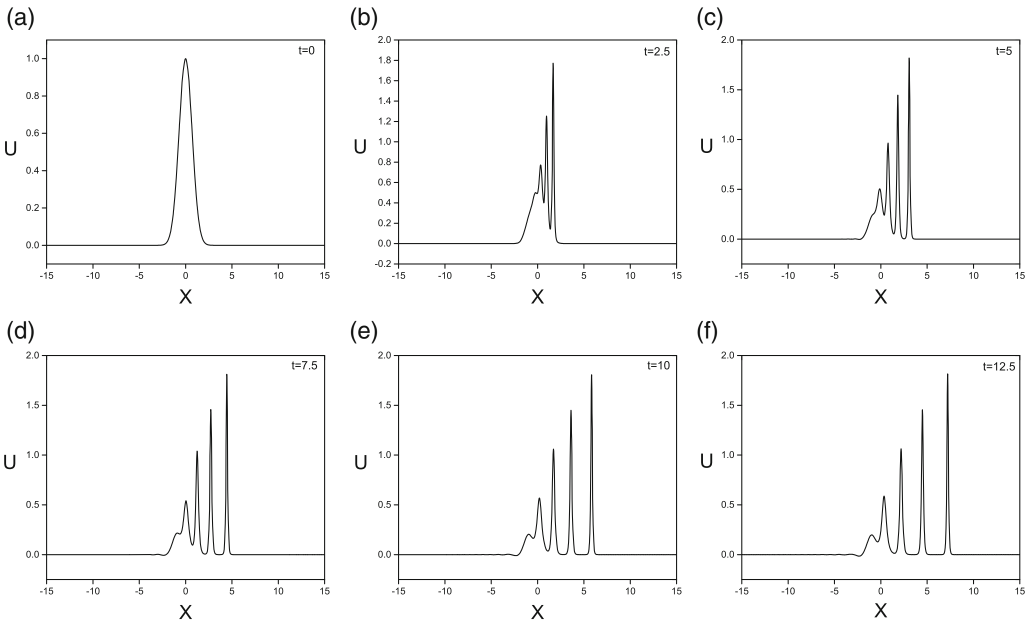

Figure 9. Simulations of Maxwellian initial condition for $\mu = 0.0025$: (**a**) $t = 0$, (**b**) $t = 2.5$, (**c**) $t = 5$, (**d**) $t = 7.5$, (**e**) $t = 10$ and (**f**) $t = 12.5$.

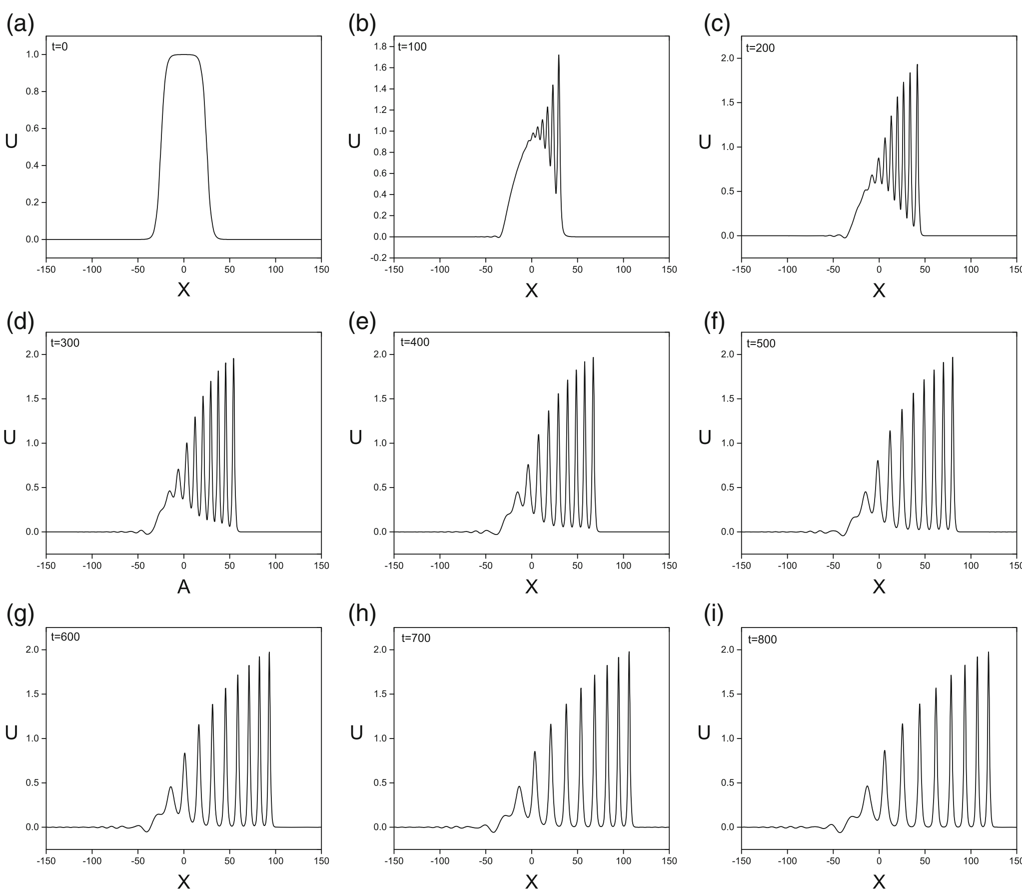

Figure 10. Simulations of the train of solitons: (**a**) $t = 0$, (**b**) $t = 100$, (**c**) $t = 200$, (**d**) $t = 300$, (**e**) $t = 400$, (**f**) $t = 500$, (**g**) $t = 600$, (**h**) $t = 700$ and (**i**) $t = 800$.

Table 9. Invariants for tanh initial condition: $\varepsilon = 0.2$ and $\mu = 0.1$.

	QCN-DQM (present) $\Delta t = 0.05$ and $N = 801$			Quad. FEM [29] $\Delta t = 0.05$ and $N = 750$		
t	I_1	I_2	I_3	I_1	I_2	I_3
0	50.000210	45.000450	40.434230	50.000244	45.000481	40.433926
100	50.000210	45.000490	40.432260	49.983517	44.910309	39.909645
200	50.000270	45.000950	40.425900	49.935287	44.674023	38.445984
300	50.000610	45.002050	40.424920	49.913094	44.565525	37.815990
400	50.000530	45.004010	40.428280	49.905308	44.536327	37.681885
500	50.001190	45.008430	40.437940	49.903107	44.530098	37.638954
600	50.002360	45.008120	40.436530	49.902920	44.530876	37.612217
700	50.005220	45.005430	40.430750	49.908508	44.535641	37.582287
800	50.000770	45.007310	40.434640	49.920536	44.540688	37.587090

5. Conclusion

In this study, the approximate solutions of the mKdV equation have been obtained using QCN-DQM. All the weighting coefficients are obtained directly by using quintic B-splines. After the discretisation of the mKdV equation with forward difference formulae and Crank–Nicolson scheme, the Rubin and Graves linearisation technique is used. After the implementation of DQM on the equation, the linear equation system is obtained and solved by Gauss method easily. Five well-known test problems have been solved. It can be seen obviously from a comparison of the present results and earlier works [26–30] that QCN-DQM can be effectively used for long runs of the mKdV equation. It is observed that conservation laws are reasonably satisfied for all the test problems given in the present paper. The obtained numerical results and comparison of the error norms L_2 and L_∞ and also the three invariants show that QCN-DQM can achieve high accuracy and good conservation properties. It can be concluded that the present approximation is an effective and efficient method for solving the mKdV equation and can also be used for numerical solutions of other problems.

References

[1] W X Ma and Y Zhou, *J. Diff. Equ.* **264**, 2633 (2018)
[2] W X Ma, *J. Geom. Phys.* **133**, 10 (2018)
[3] W X Ma, X Young and H Q Zhang, *Comput. Math. Appl.* **75**, 289 (2018)
[4] J Y Yang, W X Ma and Z Qin, *Anal. Math. Phys.* **8**, 427 (2018)
[5] J Y Yang, W X Ma and Z Qin, *East Asia J. Appl. Math.* **8**, 224 (2018)
[6] R M Miura, *SIAM Rev.* **18**, 412 (1976)
[7] W Hereman and A Nuseir, *Math. Comput. Simul.* **43**, 13 (1997)
[8] M J Ablowitz and P A Clarkson, *Solitons, nonlinear evolution equations and inverse scattering* (Cambridge University Press, Cambridge, 1991)
[9] M J Ablowitz and H Segur, *Solitons and inverse scattering transform* (SIAM, Philadelphia, 1981)
[10] R Bullough and P Caudrey, *Solitons: Topics in current physics* (Springer, Berlin, 1980) Vol. 17
[11] P G Drazin and R S Johnson, *Solitons: An introduction* (Cambridge University Press, Cambridge, 1996)
[12] R M Miura, *J. Math. Phys.* **9**, 1202 (1968)
[13] T Nagatani, *Physica A* **264**, 581 (1999)
[14] J Zhou, Z K Shi and J L Cao, *Physica A* **396**, 77 (2014)
[15] C S Gardner, J M Greene, M D Kruskal and M R Miura, *Phys. Lett. A* **19**, 1095 (1967)
[16] C H Su and C S Gardner, *J. Math. Phys.* **10**, 536 (1969)
[17] M Salahuddin, *Plasma Phys. Control. Fusion* **32**, 33 (1990)
[18] W X Ma and Y You, *Trans. Am. Math. Soc.* **357(5)**, 1753 (2004)
[19] A Başhan, *Turkish J. Math.* **42**, 373 (2018)
[20] O E Hepson, A Korkmaz and I Dag, *Pramana – J. Phys.* **91**: 59 (2018)
[21] A Başhan, Y Uçar, N M Yağmurlu and A Esen, *J. Phys. Conf. Ser.* **766**, 012028 (2016)
[22] A Wazwaz, *Commun. Nonlinear Sci. Numer. Simul.* **13**, 331 (2008)
[23] A H Salas, *Appl. Math. Comput.* **216**, 2792 (2010)
[24] D Kaya, *Commun. Nonlinear Sci. Numer. Simul.* **10**, 693 (2000)
[25] L R T Gardner, G A Gardner and T Geyikli, *Comput. Methods Appl. Mech. Eng.* **124**, 321 (1995)
[26] A Biswas and K R Raslan, *Phys. Wave Phenom.* **19(2)**, 142 (2011)
[27] T Ak, S B G Karakoç and A Biswas, *Sci. Iran B* **24(3)**, 1148 (2017)
[28] T Ak, S B G Karakoç and A Biswas, *Iran. J. Sci. Technol. Trans. Sci.* **41**, 1109 (2017)
[29] T Geyikli, *Finite element studies of the modified KdV equation*, Doctoral dissertation (University College of North Wales, Bangor, UK, 1994)
[30] G A Gardner, A H A Ali and L R T Gardner, *Numer. Methods Eng.* **1**, 590 (1990)

[31] R Bellman, B G Kashef and J Casti, *J. Comput. Phys.* **10**, 40 (1972)
[32] R Bellman, B G Kashef, E S Lee and R Vasudevan, *Computers and mathematics with applications* (Pergamon, Oxford, 1976) Vol. 1, p. 371
[33] J Cheng, B Wang and S Du, *Int. J. Solids Struct.* **42**, 6181 (2005)
[34] C Shu and Y L Wu, *Int. J. Numer. Methods Fluids* **53**, 969 (2007)
[35] A G Striz, X Wang and C W Bert, *Acta Mech.* **111**, 85 (1995)
[36] I Bonzani, *Comput. Math. Appl.* **34**, 71 (1997)
[37] A Korkmaz and I Dağ, *Int. J. Comput.-Aided Eng. Softw.* **28(6)**, 654 (2011)
[38] A Başhan, S B G Karakoç and T Geyikli, *Kuwait J. Sci.* **42(2)**, 67 (2015)
[39] A Başhan, Y Uçar, N M Yağmurlu and A Esen, *Eur. Phys. J. Plus* **133**, 12 (2018)
[40] S B G Karakoç, A Başhan and T Geyikli, *Sci. World J.* **2014**, 1 (2014)
[41] R C Mittal and R K Jain, *Appl. Math. Comput.* **218**, 7839 (2012)
[42] A Başhan, N M Yağmurlu, Y Uçar and A Esen, *Chaos Solitons Fractals* **100**, 45 (2017)
[43] A Başhan, N M Yağmurlu, Y Uçar and A Esen, *Int. J. Mod. Phys. C* **29(6)**, 1850043 (2018)
[44] P M Prenter, *Splines and variational methods* (John Wiley, New York, 1975)
[45] S G Rubin and R A Graves, *A cubic spline approximation for problems in fluid mechanics*, Technical Report (National Aeronautics and Space Administration, Washington, 1975)